Applied Catalysis A, General 559 (2018) 138–145

Contents lists available at ScienceDirect

Applied Catalysis A, General

journal homepage: www.elsevier.com/locate/apcata

Fabrication of MIL-101(Cr/Al) with flower-like morphology and its catalytic performance

Xinnian Xia[a,*], Yingzhuang Xu[a], You Chen[a], Yutang Liu[b], Yanbing Lu[a], Luhua Shao[a]

[a] College of Chemistry and Chemical Engineering, Hunan University, Changsha 410082, PR China
[b] Key Laboratory of Environmental Biology and Pollution Control (Hunan University), Ministry of Education, Changsha 410082, PR China

ARTICLE INFO

Keywords:
Metal organic frameworks
Flower-like morphology
Hydroxyalkylation
MIL-101(Cr/Al)
Bisphenol F

ABSTRACT

The morphology and structure of metal organic frameworks (MOFs) are closely related to their properties. Herein, a flower-like morphology MOF (named as MIL-101(Cr/Al)$_{A\text{-}f}$) was rationally designed in a acid-free environment and the Al^{3+} was transformed into the framework by the substitution process of cation exchange. During the preparation process of MIL-101(Cr/Al)$_{A\text{-}f}$, we found that the acidity of the reaction mixture could regulate the morphology of MIL-101(Cr/Al)$_{A\text{-}f}$ by adjusting the coordination of the metal clusters and the ligand chains. The catalytic performance of MIL-101(Cr/Al)$_{A\text{-}f}$ was evaluated by the hydroxyalkylation of phenol with formaldehyde. Due to the larger surface area and high-density sites, MIL-101(Cr/Al)$_{A\text{-}f}$ showed a higher catalytic activity than the octahedron morphology MIL-101(Cr/Al)$_{A\text{-}0.5}$ which was prepared with traditional method in acidic environment. In approximately equal Al^{3+} content, the MIL-101(Cr/Al)$_{A\text{-}f}$ showed a remarkably high yield (97.1%) and a excellent selectivity (98.3%) to bisphenol F at 60 °C for 30 min. Finally, a possible mechanism for the synthesis of bisphenol F was proposed and the hydroxyalkylation of phenol with formaldehyde to bisphenol F was fitted by the Langmuir-Hinshelwood kinetic model.

1. Introduction

Porous solid materials are of great importance for catalysis [1], gas storage [2], liquid separation processes [3], sensing [4], drug delivery [5], luminescence [6] and magnetism [7]. Continuous efforts from both industry and academia have been committed to the search for novel types of porous materials. Among the various candidates explored in the past two decades, MOFs have attracted a wide range of interests due to its tailorable and versatile structures, extremely high surface areas and permanent nanoscale porosities [8–10]. As a relatively novel crystalline porous material, MOFs are promising for applications in the fields of catalysis [11–13]. The presence of coordinatively unsaturated metal sites in MOFs allows its use as a Lewis acid and, more important, allows its postfunctionalization via grafting of active species. Particularly, these high-density unsaturated metal sites can be uniformly distributed throughout the MOFs. Regarding the functionalization of MOFs, there have been four main approaches: a) functionalization of the organic linkers by pre-modified [14,15], b) functionalization of the linker sites or organic ligands by post-covalent modification [16,17], c) post-grafting of coordinatively unsaturated sites with chelators or metal clusters [18], (d) synthesis of multi-metal frameworks by one-step method [19–22]. Chui et al. reported that the ligands can be replaced by other chains, such as pyridine [23]. It has been also reported that the cavities of framework can be modified by chemical modification without change of the original crystal structure. Kitagawa and co-workers proposed that the introduction of functional groups decorates the sites of the framework. Cristina P. Krap and co-workers reported the incorporation of metal ions into the metal-organic frameworks by one-pot for catalysis [19]. In addition, various morphologies can be obtained by different synthetic approaches such as the Kirkendall effect, template method, microwave radiation method, chemical etching, ions doping and chemical vapor deposition method [24–30]. In order to maximize the structure advantage and realize beneficial functionalities, the rational design of morphology with high-density accessible sites is highly desirable.

We chose MIL-101-Cr as the platform material because of its high water/chemical stability and readiness for functionalization via post-synthetic modification methods, and the morphology of MIL-101-Cr can be controlled by adjusting parameters during the preparation process. This hybrid material is composed of supertetrahedral building units, which are formed from trimeric metal octahedron clusters and rigid terephthalate ligands [31]. The resulting three-dimensional cage material possesses two types of quasispherical mesoporous cages formed by hexagonal windows and pentagonal windows, respectively. In

* Corresponding author at: College of Chemistry and Chemical Engineering, Hunan University, Lushan South Road, Yuelu District, Changsha 410082, PR China.
E-mail address: xnxia@hnu.edu.cn (X. Xia).

https://doi.org/10.1016/j.apcata.2018.04.020
Received 23 January 2018; Received in revised form 18 April 2018; Accepted 19 April 2018
Available online 22 April 2018
0926-860X/

addition, the presence of open metal sites and regular frameworks in MIL-101 contributes to postfunctionalization via grafting of active species [32]. The fully accessible porosity, the favorable structural morphology, together with a high chemical and thermal stability make MIL-101 an excellent potential for catalytic purposes.

In this paper, a novel strategy has been proposed for preparing MIL-101(Cr/Al)$_{A\text{-}f}$ in a acid-free environment and a substitution process by cation exchange was carried out to transform the Al^{3+} into MOFs. We compared the catalytic properties of the prepared MIL-101(Cr/Al)$_{A\text{-}f}$ with the MIL-101(Cr/Al)$_{A\text{-}0.5}$ in hydroxyalkylation of phenol with formaldehyde. In addition, the effect of acidity on the morphology of the framework during the preparation process was investigated. The MIL-101(Cr/Al)$_{A\text{-}f}$ exhibited a excellent catalytic activity due to its unique morphology, which was supported by BET, SEM and TEM. Finally, a possible mechanism for the synthesis of bisphenol F was proposed and the hydroxyalkylation of phenol with formaldehyde was fitted by the Langmuir-Hinshelwood kinetic model.

2. Experimental section

2.1. Chemicals

All chemicals were provided from commercially available resources and were studied without further processing. Chromium nitrate nonahydrate ($Cr(NO_3)_3{\cdot}9H_2O$), aluminum chloride hexahydrate, nitric acid, terephthalic acid (BDC, 98%), N,*N*-dimethylformamide (DMF, 99%), formaldehyde (37–40%) and phenol were obtained from Sinopharm Chemical Reagent Co. Ltd., China.

2.2. Synthesis of MIL-101(Cr/Al)$_{A\text{-}X}$

Typical synthetic process was carried out via hydrothermal synthesis and described as follows: BDC (1.66 g, 10 mmol), $Cr(NO_3)_3{\cdot}9H_2O$ (4.0 g, 10 mmol), deionized water (30 mL) and nitric acid from 0 to 0.5 g were mixed at room temperature, and then sonicated for 30 min. The mixture was transferred into a 50 mL Teflon-lined autoclave and heated at 220 °C for 18 h. The suspension was centrifuged and the precipitate was washed with DMF and ethanol. The obtained product was dried at 150 °C for 12 h. 1 g of sample was refluxed in 50 mL of 0.3 m/L $AlCl_3$ aqueous solution at 70 °C for 24 h. Then solid was separated by centrifugation and washed twice with ethanol. Finally, the samples were vacuum-dried at 150 °C for 12 h, and labeled as MIL-101(Cr/Al)$_{A\text{-}X}$, where X represents the quality of nitric acid in the preparation process (0.5 g, 0.3 g, 0.1 g and free).

2.3. Characterization techniques

The crystalline phases of the products were examined by X-ray diffraction (Bruker D8 Advance diffractometer) with Cu Ka radiation (working at 40 kV and current 40 mA). Diffraction data were recorded in the 2 h range from 1° to 8° and 10° to 80° (increment: 0.5°). The unit cell parameters were calculated with a standard least squares refinement technique. NH_3-TPD analysis was performed with a Micromeritics AutoChem II 2920 V3.05 instrument. Prior to analysis, the catalyst (100 mg) was enclosed in a quartz tube and treated at 300 °C under helium flow of 30 mL min^{-1} for 1 h. The magic angle spinning (MAS) NMR analysis was performed by a Bruker Avance-400 with a 5 mm zirconia rotor and a spinning frequency of 11 kHz. Spectra for ^{27}Al was obtained. The porosity was analyzed by N_2 adsorption at 77 K using an ASAP 2010 sorption system. UV–vis diffuse reflectance spectra were recorded at a Perkin–Elmer Lambda 900 spectrophotometer under 200–800 nm. The binding energies of C, O, Cr and Al of the composite microspheres were detected on X-ray photoelectron spectroscopy (Thermo Fisher, USA) using an Al-KX-ray source. Scanning electron microscopy (SEM) micrographs were obtained on a Hitachi S4800 microscope operated at 30 kV. Transmission electron microscopy (TEM) and elemental mapping analysis were collected using a high-resolution transmission electron microscope (HRTEM, TECNAI F20). Energy-dispersive X-ray (EDX) analysis was used to determine the chemical composition of the samples. Thermogravimetric analysis (TGA) was recorded on a Mettler-Toledo 1600HT thermoanalyzer under a nitrogen atmosphere at a heating rate of 10 °C min^{-1}. The concentration of aluminum was monitored by an atomic absorption spectrophotometer (Z-2000, Hitachi, Japan).

2.4. Catalytic activity tests

Hydroxyalkylation of phenol with formaldehyde to bisphenol F was carried out in reactor with magnetic stirring. Typical experimental processes were summarized as follows: 0.465 g (5.7 mmol) of formaldehyde solution, 8.12 g of phenol and 0.12 g of catalyst were added into the reactor and the reaction mixture was heated to the desired temperature. After a certain time interval, 0.03 g of the suspension was taken out and then diluted with 10 mL of methanol. The composition of the product was confirmed by HPLC with a Shimadzu LC-20AT system connected with a SPD-20A UV/Vis detector and a Phenomenex Luna C18 column (250 × 4.6 mm, 5 mm); A mixture of methanol and water with 65:35 v/v was used as the mobile phase with a constant flow rate of 0.6 mL/min. The injective volume of the sample was 100 μL.

The yield and selectivity of bisphenol F are calculated on the basis of formaldehyde. The calculation equations are as follows:

$$\text{Yield}(\%) = \frac{\text{Moles of bisphenol F formed}}{\text{Expected moles of bisphenol F formed based on formaldehyde consumed}} \times 100\%$$

$$\text{Selectivity}(\%) = \frac{\text{Moles of bisphenol F formed}}{\sum \text{Moles of all the products}} \times 100\%$$

The synthetic route for the formation of bisphenol F by hydroxyalkylation of phenol with formaldehyde is shown in Scheme 1.

3. Results and discussion

3.1. Catalyst characterizations

The morphological evolution of MIL-101(Cr/Al)$_{A\text{-}X}$ was conducted by scanning electron microscopy (SEM) and transmission electron microscopy (TEM). MIL-101(Cr/Al)$_{A\text{-}0.5}$ (Fig. 1a and b) exhibits single octahedron morphology with a size around 300 nm, while the flower-like morphology of MIL-101(Cr/Al)$_{A\text{-}0.3}$ begins to appear in the vicinity of the octahedron morphology (Fig. S1a–c). With the acidity weakening, more deprotonated carboxyl groups are generated to accelerate coordination with metal clusters. The appearance of mixed octahedron/flower-like morphologies may be attributed to the heterogeneous nucleation in the patterns of MIL-101(Cr/Al)$_{A\text{-}0.3}$. During the heterogeneous nucleation process, the increased deprotonated carboxyl groups firstly form flower-like morphology and the remained deprotonated carboxyl groups with low concentration form octahedron morphology. The particle size of octahedron morphology in MIL-101(Cr/Al)$_{A\text{-}0.3}$ (~150 nm) is about half smaller than that of MIL-101(Cr/Al)$_{A\text{-}0.5}$ with single octahedron morphology, which may due to the presence of flower-like morphology in their adjacent areas. In addition, the particle size of original MIL-101(Cr)$_{A\text{-}X}$ is investigated. The particle size of flower-like MIL-101(Cr)$_{A\text{-}f}$ is slightly larger than that of octahedron MIL-101(Cr)$_{A\text{-}0.5}$ (Fig. S2), which is consistent with the reference [33]. As shown in Table S1 and Fig. S3, the average particle size of MIL-101(Cr)$_{A\text{-}X}$ is analysed using a GaussAmp model. With the decrease of acidity, the number of the deprotonated carboxyl groups of terephthalic acid increases, which speeds up the rate of coordination with metal ions. The increase of the coordination rate makes the coordination tend to irregular and outward growth, leading to larger particles. With the decrease of acid from 0.3 to 0.1 g, the growth of flower-like morphology is easier (Fig. S1d–f). When there is no nitric acid, we get a nearly perfect flower-like morphology (Fig. 1c–e). The HRTEM images (Fig. 1f)

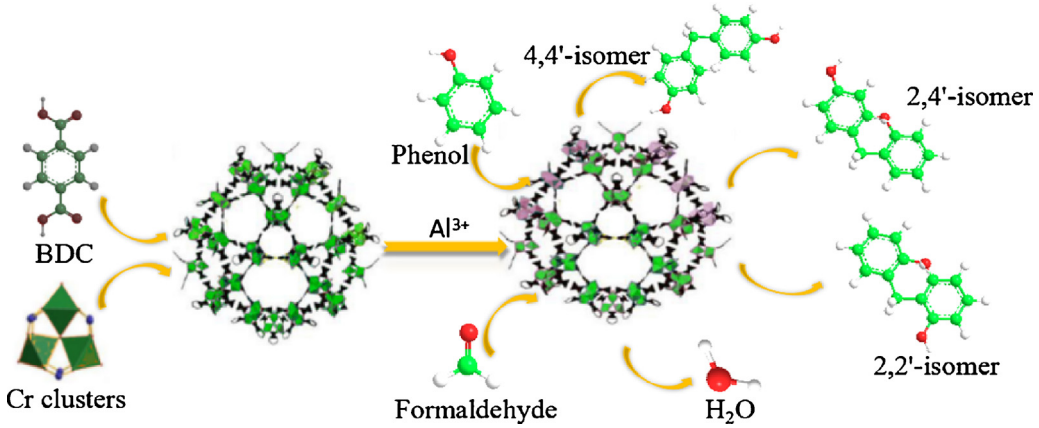

Scheme 1. Hydroxyalkylation of phenol with formaldehyde to bisphenol F.

further reveal that the surface of the 'flower-like' is distributed with a high density of stacking faults. The interfacial spacing of flower-like morphology is determined to be 0.24 nm, corresponding to the (104) plane of CrO(OH) (PDF 09-0331), which is absent in the original octahedron morphology (Fig. S4). Fig. 1g is the corresponding fast Fourier transform (FFT) pattern of the MIL-101(Cr/Al)$_{A\text{-}f}$ samples. In addition, the elemental maps corresponding to flower-like morphology MIL-101(Cr/Al)$_{A\text{-}f}$ are depicted in Fig. 1h, confirming that the C, O, Cr, Al are of uniformly distributed in MIL-101(Cr/Al)$_{A\text{-}f}$.

Normally, each Cr or Al ion is six-coordinated by four oxygen atoms of the bidendate dicarboxylates, one μ_3O atom and one oxygen atom from the terminal water. Octahedra are related through the μ_3O oxygen atom to form the trimeric building unit. A superterahedral building unit is formed by trimeric metal cations octahedron clusters and rigid terephthalate ligands, which further constructs a three-dimensional network [32]. In the preparation process, the amount of acid influences the coordination of MIL-101(Cr/Al)$_{A\text{-}X}$ by adjusting the deprotonation of BDC. During crystal formation, acid has a double function: it slows down the hydrolysis of metal cations and counteracts the deprotonation of the dissolved carboxylic acids [34]. In our study, the acidic solution reduces the deprotonation capacity of carboxylic acids during the preparation process of catalysts, and then slows the coordination rate of metal ions with ligand chains. Therefore, the system have more opportunities to form regular structure morphology. With the amount of acid decreasing, the morphology tends to be irregular, resulting that a few flower-like morphologies gradually nucleates in the vicinity of the octahedron morphology. When there is no nitric acid, we get a nearly perfect flower-like morphology. The formation mechanism of the MIL-101(Cr/Al)$_{A\text{-}f}$ with flower-like morphology is explored and illuminated in Scheme 2. The special morphology of MIL-101(Cr/Al)$_{A\text{-}f}$ could supply huge surface areas and a large number of accessible active sites, which is closely related to the catalytic performance [35]. The elemental analysis spectroscopy (Fig. 2) reveals that the Al^{3+} content of MIL-101(Cr/Al)$_{A\text{-}0.5}$ and MIL-101(Cr/Al)$_{A\text{-}f}$ are similar, but the catalytic activity is lower than the latter (as shown in the section of 3.2). This phenomenon further illustrates that the morphology of catalysts is critical for the reaction process.

The structure and composition of the MIL-101(Cr)$_{A\text{-}f}$ and MIL-101(Cr/Al)$_{A\text{-}X}$ were confirmed by X-ray diffraction (XRD) and the results are shown in Fig. 3. The low-angle X-ray diffraction profiles of the samples in Fig. 3a indicate no obvious collapse of the intrinsic structure of MIL-101(Cr)$_{A\text{-}f}$ after the immobilization of Al^{3+}. The as-synthesized MIL-101(Cr/Al)$_{A\text{-}0.5}$ exhibits characteristic peaks of CrO(OH) (PDF No. 25-1497) at around 17.89°, 21.69°, 26.93°, and 41.74°, and characteristic peaks 22.84°, 26.92° and 35.0° also presenting in MIL-101(Cr/Al)$_{A\text{-}0.5}$ belong to AlO(OH) (PDF No. 48-0890). The XRD pattern with characteristic peaks at around 19.98°, 37.33°, 48.99°, 62.26° and 66.02° is detected for MIL-101(Cr/Al)$_{A\text{-}f}$, which is in accordance with CrO(OH) (PDF No. 09-0331). The characteristic peak at 48.99° is ascribed to the characteristic peak of AlO(OH) (PDF No. 49-0133) in MIL-101(Cr/Al)$_{A\text{-}f}$. The acid concentration during the preparation process affects the crystal growth and further influences the catalytic performance of the framework.

N_2 adsorption-desorption isotherms of the MIL-101(Cr)$_{A\text{-}f}$ and MIL-101(Cr/Al)$_{A\text{-}X}$ are shown in Fig. 4. According the IUPAC classification, the N_2 isotherms for MIL-101(Cr)$_{A\text{-}f}$ and MIL-101(Cr/Al)$_{A\text{-}X}$ are founded to be of type I and IV, respectively [32]. At very low relative pressures ($P/P_0 < 0.05$), only the supertetrahedra are filled. As pressure increases, the medium ($P/P_0 = 0.15$) and later ($P/P_0 = 0.20$) the large cavities are filled [31]. As shown in Table 1, the specific surface area of MIL-101(Cr/Al)$_{A\text{-}X}$ reduces compared to MIL-101(Cr)$_{A\text{-}f}$. The specific surface area of MIL-101(Cr/Al)$_{A\text{-}f}$ is 2037 m^2/g, while that of MIL-101(Cr/Al)$_{A\text{-}0.5}$ is just 1873 m^2/g. The phenomenon may be due to the fact that the specific surface area of the flower-like is larger than that of the octahedron with similar size [36]. In addition, the pore size of MIL-101(Cr/Al)$_{A\text{-}f}$ is larger than that of MIL-101(Cr/Al)$_{A\text{-}0.5}$ (Fig. 4b). The unit cell parameters of the MIL-101(Cr)$_{A\text{-}f}$ before and after modification are investigated and shown in Fig. S5. Incorporation of Al in the framework of MIL-101(Cr)$_{A\text{-}f}$ decreases the unit cell parameters along the a-axes. The cell parameters of 9.69% aluminum substituted MIL-101(Cr)$_{A\text{-}f}$ is 20.81 Å, whereas that of MIL-101(Cr)$_{A\text{-}f}$ is 21.48 Å. The slightly change in the unit cell parameter could be anticipated because the ionic radii of the Al and Cr ions are 0.535 Å and 0.615 Å, respectively [37].

UV-Vis spectroscopy is a sensitive tool for probing any changes in the composition of the secondary structural. Visible-light absorption is due to the d–d transitions of the metal trimers, while UV absorption corresponds to the π–π transitions of the linkers. As shown in Fig. 5, the characteristic absorption peaks of MIL-101(Cr/Al)$_{A\text{-}0.5}$ appear at 445 nm and 602 nm, while the characteristic absorption peaks of MIL-101(Cr/Al)$_{A\text{-}f}$ appear at 442 nm and 601 nm, respectively. Compared with MIL-101(Cr), incorporation of Al in the framework leads to the change of characteristic peaks, which is consistent with the literature [36]. The shift of peaks is due to the fact that different metal ions have different electronic configurations, and Al is a p-metal that should have an effect on the d-d transition of the metal chromium sites. Besides, the XPS spectrum of MIL-101(Cr/Al)$_{A\text{-}f}$ shown in Fig. S6 demonstrates that Al^{3+} presents in the framework. The ^{27}Al NMR spectrum is shown in Fig. S7. The presence of one single signal at $\delta = 0$ ppm demonstrates that the Al in the sample has an octahedral coordination [38].

The TG pattern of the samples is shown in Fig. 6 and used to quantify the thermal degradation of MIL-101(Cr/Al)$_{A\text{-}0.5}$ and MIL-101(Cr/Al)$_{A\text{-}f}$. It can be seen that the thermal stable temperature of both MIL-101(Cr/Al)$_{A\text{-}f}$ and MIL-101(Cr/Al)$_{A\text{-}0.5}$ can reach 400 °C. The weight loss of the samples is obviously divided into two stages. The first stage of weight loss at 100 °C is related to the removal of water

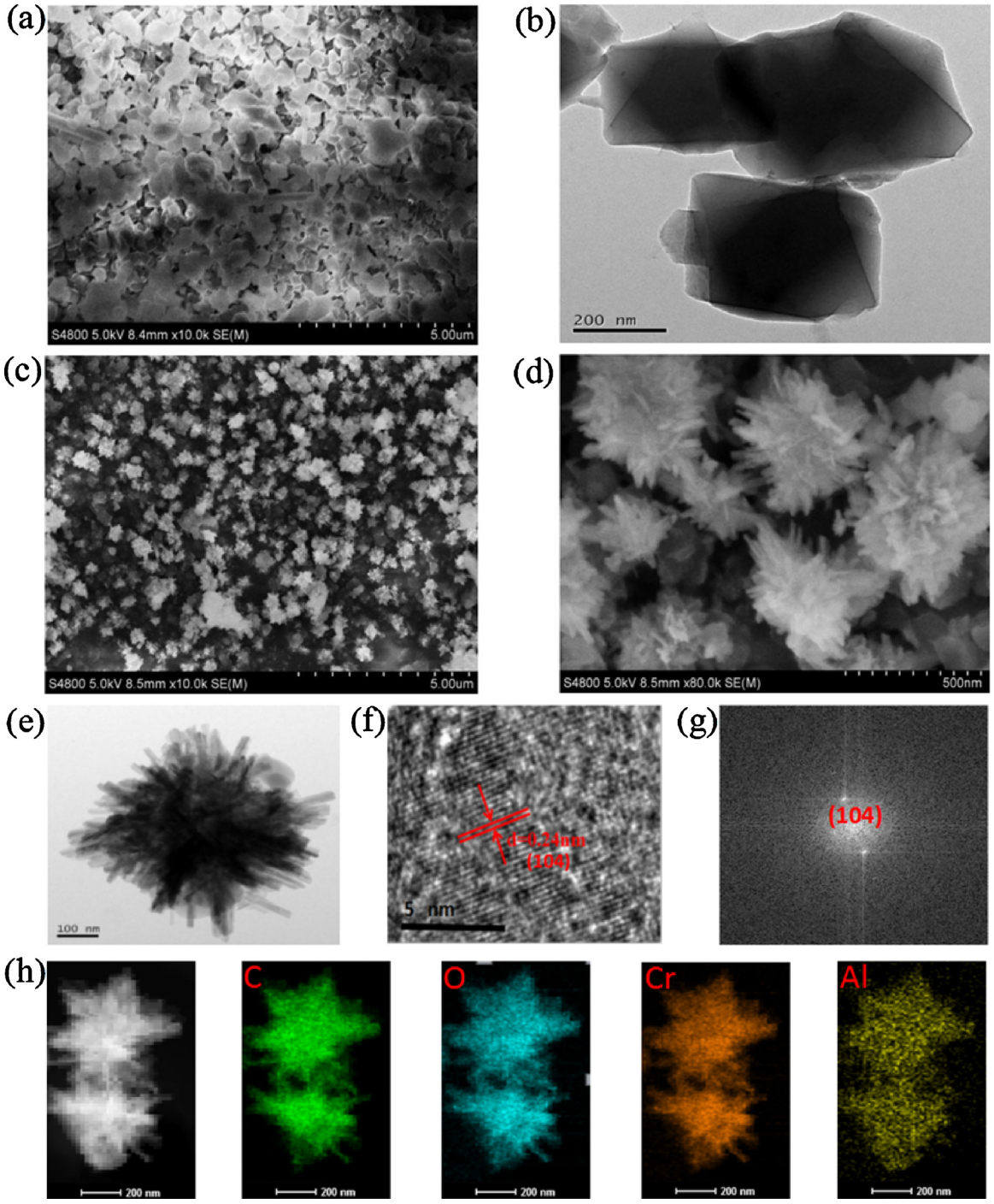

Fig. 1. (a) SEM and (b) TEM images of MIL-101(Cr/Al)$_{A\text{-}0.5}$; (c, d) SEM, (e) TEM, (f) HRTEM, (g) FFT and (h) Element mappings images of MIL-101(Cr/Al)$_{A\text{-}f}$.

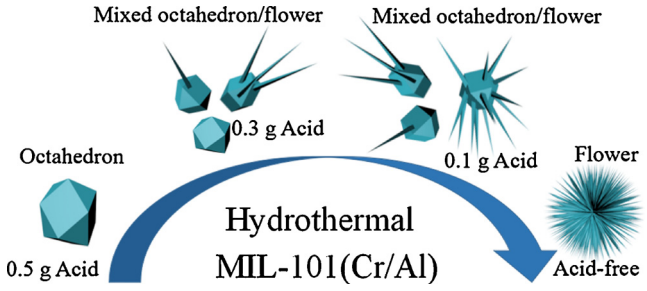

Scheme 2. Proposed plausible mechanism for morphological evolution.

molecules, while the weight loss up to 400 °C may correspond to decomposition of the three-dimensional frameworks [39].

3.2. The catalytic performances of MIL-101(Cr/Al)$_{A\text{-}f}$

The properties of catalysts are evaluated by the hydroxyalkylation of phenol with formaldehyde to bisphenol F. As shown in Table 2, MIL-101(Cr)$_{A\text{-}f}$ shows a lower catalytic activity for the synthesis of bisphenol F (5.9%) compared to MIL-101(Cr/Al)$_{A\text{-}X}$, although the former has a relatively large pore size. It's reported that the hydroxyalkylation of phenol with formaldehyde strongly depends on the strength of the acid and the structure of the catalyst [40]. Due to the Al-containing metal organic framework has stronger acidity than the Cr-containing

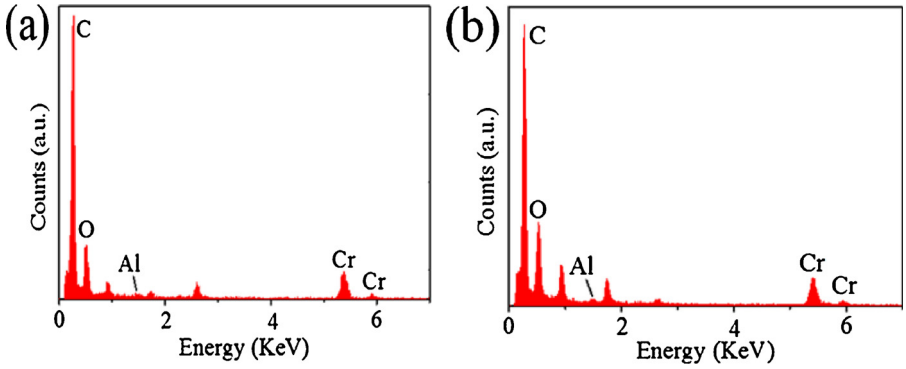

Fig. 2. EDX spectrum of (a) MIL-101(Cr/Al)$_{A\text{-}f}$ and (b) MIL-101(Cr/Al)$_{A\text{-}0.5}$.

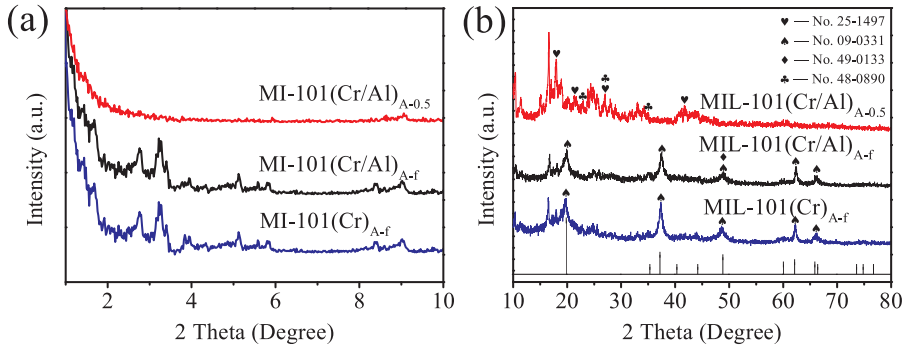

Fig. 3. XRD patterns of MIL-101(Cr)$_{A\text{-}f}$ and MIL-101(Cr/Al)$_{A\text{-}X}$.

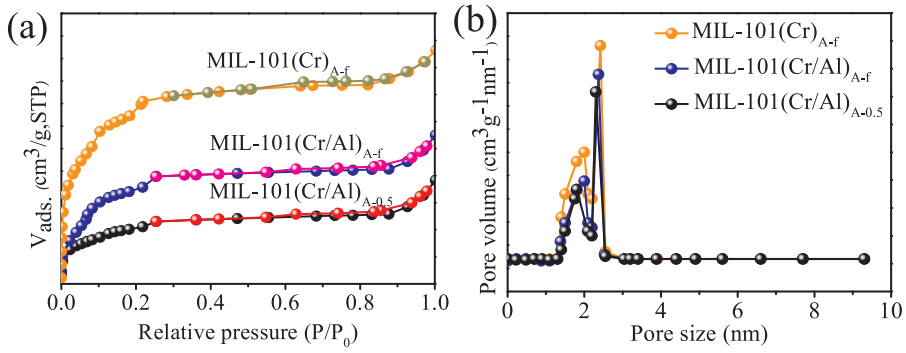

Fig. 4. (a) N_2 adsorption-desorption curves of MIL-101(Cr)$_{A\text{-}f}$ and MIL-101(Cr/Al)$_{A\text{-}X}$; (b) pore size distributions of MIL-101(Cr)$_{A\text{-}f}$ and MIL-101(Cr/Al)$_{A\text{-}X}$.

Table 1
Structural data of MIL-101(Cr)$_{A\text{-}f}$ and MIL-101(Cr/Al)$_{A\text{-}X}$.

Samples	Surface area ($m^2\,g^{-1}$)	Pore volume ($cm^3\,g^{-1}$)	Pore size (nm)
MIL-101(Cr/Al)$_{A\text{-}0.5}$	1873	1.37	1.7, 2.2
MIL-101(Cr/Al)$_{A\text{-}f}$	2037	1.41	1.9, 2.4

framework, the catalytic activity of the MIL-101(Cr/Al)$_{A\text{-}X}$ is significantly enhanced in the synthesis of bisphenol F [41,42]. The catalytic activity of MIL-101(Cr/Al)$_{A\text{-}f}$ and MIL-101(Cr/Al)$_{A\text{-}0.5}$ with the similar amount of Al^{3+} is compared here. The results reveal that MIL-101(Cr/Al)$_{A\text{-}f}$ (97.1%) has better catalytic activity than MIL-101(Cr/Al)$_{A\text{-}0.5}$ (88.7%), which is attributed to more acidic sites in the MIL-101(Cr/Al)$_{A\text{-}f}$ (Fig. S8). The sites at the edges and corners are generally considered to be more accessible and more active than the sites in the middle of platelets for acidic catalyzed reactions [35]. The presence of high-density acidic sites at the edges of the flower-like allows MIL-101(Cr/Al)$_{A\text{-}f}$ to have more favorable structures than the octahedron

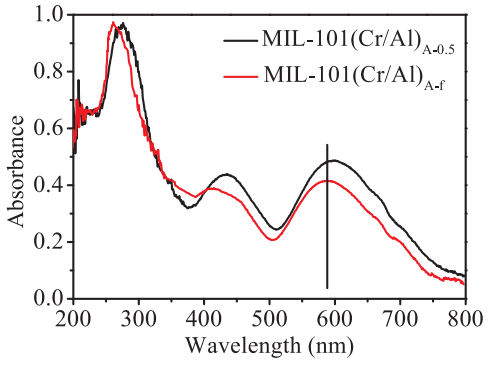

Fig. 5. UV–Vis spectra of MIL-101(Cr/Al)$_{A\text{-}0.5}$ and MIL-101(Cr/Al)$_{A\text{-}f}$.

MIL-101(Cr/Al)$_{A\text{-}0.5}$, thereby it enables the catalytic reaction proceeding smoothly. As shown in Fig. S9, The influences of various reaction parameters like reaction temperature, reaction time, mole ratio and catalyst concentration on the hydroxyalkylation of phenol with

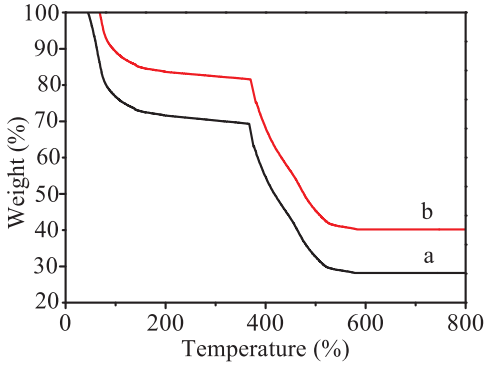

Fig. 6. TG patterns of (a) MIL-101(Cr/Al)$_{A-0.5}$, (b) MIL-101(Cr/Al)$_{A-f}$.

formaldehyde to bisphenol F over MIL-101(Cr/Al)$_{A-f}$ have also been investigated. The 4,4 isomer of bisphenol F may be kinetically controlled while the 2,4 and 2,2 isomer are thermodynamically controlled. The 4,4 isomer of bisphenol F is readily produced at low temperature and the 4,4 isomer is transformed to the 2,4 and 2,2 isomer at high temperature. Compared with MIL-101(Cr/Al)$_{A-f}$, bisphenol F synthesized in hydroxyalkylation reaction by MIL-101(Cr/Al)$_{A-0.5}$ has slightly higher 4,4 isomers and slightly lower 2,4 isomers (Fig. S10). The recyclability of MIL-101(Cr/Al)$_{A-f}$ is shown in Fig. S11. It is observed that the morphology of the catalyst after recycling maintains flower-like (Fig. S12). The recovery of MIL-101(Cr/Al)$_{A-f}$ after 3 cycles calculated based on the leaching amount of aluminum ions was shown in Fig. S11. The contribution of homogeneous aluminum ions to the catalytic performance is almost negligible, which further proves the stability of the catalyst. In view of characterization analysis and performance tests, it can be deduced that the microenvironment during the preparation process is crucial for the morphology of the framework, which further influences its catalytic activity.

In order to further investigate the effect of the inherent structure of the catalyst on the reaction performance, several catalysts are selected for the synthesis of bisphenol F. As shown in Table 2, it can be seen that MIL-101(Cr/Al)$_{A-f}$ has relatively high catalytic activity although the amount of Al^{3+} is lower than conventional Al-based catalysts. Since chemical reactions are determined by the availability of the active sites rather than the number of the active sites, the significantly enhanced catalytic activity of the MIL-101(Cr/Al)$_{A-f}$ could be mainly attributed to three factors : (i) the large pore volume and specific surface area of the MIL-101(Cr/Al)$_{A-f}$ promote the evacuation process of the substrate and product. (ii) active ingredients can be better involved in the carrier to improve its structural properties. (iii) the good interconnection of the nano-spacing in the three-dimensional cage of MIL-101(Cr/Al)$_{A-f}$ makes it easier that high-density active sites in MIL-101(Cr/Al)$_{A-f}$ can be exposed in the system. Therefore, the MIL-101(Cr/Al)$_{A-f}$ is found to be more effective in the conversion of phenol and formaldehyde, which in turn illustrates that the ionic activity and the intrinsic structure of the catalyst are two indispensable factors in the chemical process.

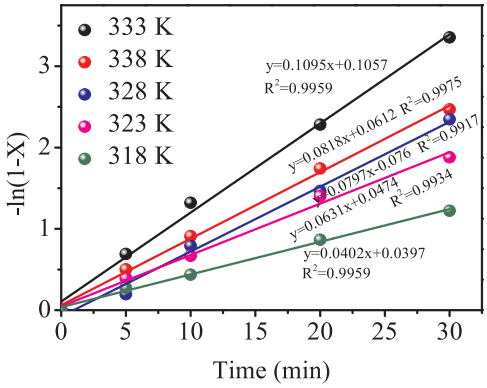

Fig. 7. Kinetic plot of -ln(1 - X) vs time. Reaction conditions: molar ratio of phenol to formaldehyde, 15:1; catalyst amount, 0.3 wt%.

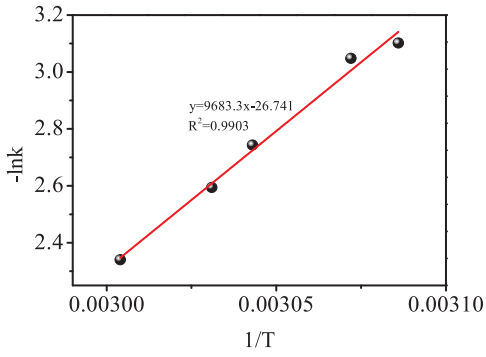

Fig. 8. Arrhenius plot of -ln k vs T^{-1}.

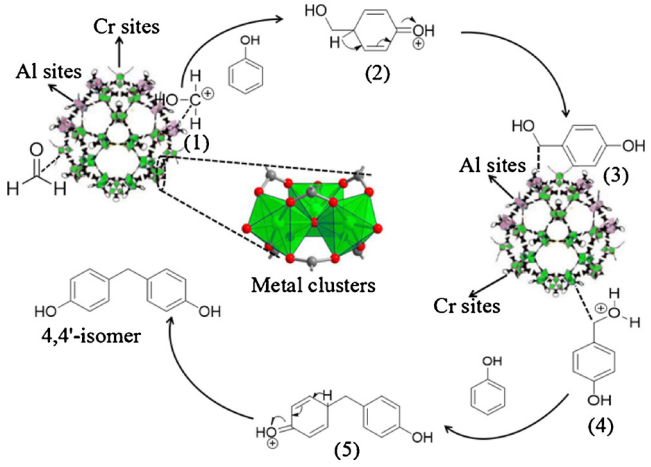

Scheme 3. Proposed plausible mechanism for hydroxyalkylation of phenol with formaldehyde to bisphenol F.

Table 2
Catalytic activities of MIL-101(Cr)$_{A-f}$, MIL-101(Cr/Al)$_{A-X}$ and other Al-based catalysts for bisphenol F. Reaction conditions: phenol/formaldehyde molar ratio, 15 : 1; catalyst concentration, 0.3 wt%; reaction temperature, 333 K; reaction time, 30 min.

Catalyst	Reaction time/min	Reaction temperatur/°C	Al conten/wt%	Yiel/%	Selectivit/%	Ref.
MIL-101(Cr)$_{A-f}$	30	60	0	5.9	96.6	This study
MIL-101(Cr/Al)$_{A-0.5}$	30	60	10.05	88.7	96.7	This study
MIL-101(Cr/Al)$_{A-f}$	30	60	9.69	97.1	98.3	This study
Al-SPC	40	60	27.2	87.3	97.6	[43]
Al-MMT	30	110	34.9	55.7	89.2	[44]
Al-MCM	240	90	30	88.3	90.7	[45]
Al-H-beta	60	90	25	91.2	91.4	[46]

3.3. Kinetics study

After validating the catalytic performance of MIL-101(Cr/Al)$_{A\text{-}f}$ in the hydroxyalkylation of phenol with formaldehyde, the experimental data are further used to establish a kinetic model based on the Langmuir-Hinshelwood mechanism. In the bimolecular equilibrium system, the concentration of phenol and formaldehyde is theoretically related to its reaction rate. The kinetic equation is written in Eq. (1), where k represents the reaction rate constant, r represents the reaction rate, t represents the reaction time, C_{phenol} represents the concentration of phenol, $C_{formaldehyde}$ represents the concentration of formaldehyde, X represents the conversion of formaldehyde, α and β represent the reaction order. Although the reaction is accompanied by the occurrence of side reactions in this system, the conversion rate of formaldehyde is approximately equal to the yield due to the high selectivity of bisphenol F. Since phenol is far more than formaldehyde, we assume that the reaction is a pseudo-first-order reaction of formaldehyde. Based on the analysis above, we have simplified the equation for the hydroxylation of phenol with formaldehyde as Eq. (2).

In order to analyze the kinetics of system, the standard first-order kinetic equation is written as Eq. (3). In addition, the Arrhenius equation is used to estimate the activation energy of the reaction system (Eq. (4)), where R represents the universal gas constant, Ea represents the activation energy, and T represents the reaction temperature of the system.

To validate the above assumptions, five straight lines are simulated at temperatures of 318 K, 323 K, 328 K, 333 K and 338 K, respectively. As shown in Fig. 7, the slope of these lines is k which shows a good linear relationship and the linearity of the plots with correlation coefficient $R^2 > 0.99$. In addition, the rate constant k increases with the increase of the temperature in a certain range, indicating that the high temperature is favorable for the reaction. It means that the rate of the hydroxyalkylation is the Langmuir-Hinshelwood type over MIL-101(Cr/Al)$_{A\text{-}f}$ with respect to the formaldehyde. The Arrhenius plot of -ln k_1 vs 1/T is shown in Fig. 8, and the activation energy is calculated to be 80.5×10^3 J/mol.

$$R = -dC/dt = kC_{phenol}^{\alpha}C_{formaldehyde}^{\beta} \quad (1)$$

$$R = -dC/dt = kC^{\alpha} \quad (2)$$

$$-\ln(1-X) = kt + b \quad (3)$$

$$\ln k = -Ea/RT + \ln k_0 \quad (4)$$

3.4. Reaction mechanism

Based on the results discussed above, a possible mechanism for hydroxyalkylation of phenol with formaldehyde is presented in Scheme 3. Firstly, the formaldehyde is activated by a proton from the MIL-101(Cr/Al)$_{A\text{-}f}$ to form hydroxymethyl carbocation (1) with release of a water molecule. Then, the hydroxymethyl carbocation interacts with the carbon atoms of phenol to form the hydroxyl oxygen cation (2) which is unstable. This is followed by a proton transfer from the carbocation to catalyst and hydroxybenzyl alcohol (3) is obtained with regeneration of the catalyst. Hydroxybenzyl alcohol is further reacted with the active acid sites of the MIL-101(Cr/Al)$_{A\text{-}f}$ to form hydroxybenzyl carbocation (4). In the final stage, the hydroxybenzyl carbocation continues to attack another carbon atom of phenol to form an unstable intermediate (5). The intermediate is easy to lose protons, and eventually the 4,4′-isomer of bisphenol F is obtained.

4. Conclusion

A flower-like MIL-101(Cr/Al)$_{A\text{-}f}$ was successfully synthesized by adjusting the acidity of the reaction mixture. The composition and morphology of the MIL-101(Cr/Al)$_{A\text{-}X}$ were characterized by XRD, ^{27}Al NMR, XPS, SEM, and TEM. We found that with an increase of acid content, the structure of the MOF attempted to form flower-like morphology. When used as the catalyst of hydroxyalkylation of phenol with formaldehyde, the MIL-101(Cr/Al)$_{A\text{-}f}$ showed a higher yield and selectivity than MIL-101(Cr/Al)$_{A\text{-}0.5}$, which were 97.1% and 98.3% respectively, while the controlled MIL-101(Cr/Al)$_{A\text{-}0.5}$ had only 88.7% and 96.7% at 60 ℃ for 30 min. The other controlled catalysts were also used to evaluate catalytic activity with the similar Al content. The large surface area and high-density sites of MIL-101(Cr/Al)$_{A\text{-}f}$ could be responsible for the excellent catalytic activity in the hydroxyalkylation of phenol with formaldehyde to bisphenol F. A possible mechanism was proposed and the hydroxyalkylation was in good agreement with the Langmuir-Hinshelwood kinetic model over MIL-101(Cr/Al)$_{A\text{-}f}$.

Acknowledgements

This research was supported by the National Natural Science Foundation of China (nos. 51672077, 51378187), and Hunan Provincial Natural Science Foundation of China (no. 2017JJ2026).

Appendix A. Supplementary data

Supplementary material related to this article can be found, in the online version, at doi: https://doi.org/10.1016/j.apcata.2018.04.020.

References

[1] M.E. Davis, Nature 417 (2002) 813–821.
[2] (a) M.P. Suh, H.J. Park, T.K. Prasad, D.W. Lim, Chem. Rev. 112 (2011) 782–835; (b) R.B. Getman, Y.S. Bae, C.E. Wilmer, R.Q. Snurr, Chem. Rev. 112 (2011) 703–723.
[3] G. Dong, H. Li, V. Chen, J. Mater. Chem. A 1 (2013) 4610–4630.
[4] L.E. Kreno, K. Leong, O.K. Farha, M. Allendorf, R.P. Van Duyne, J.T. Hupp, Chem. Rev. 112 (2012) 1105–1125.
[5] S. Keskin, S. Kızılel, Ind. Eng. Chem. Res. 50 (2011) 1799–1812.
[6] Y. Cui, Y. Yue, G. Qian, B. Chen, Chem. Rev. 112 (2011) 1126–1162.
[7] M. Kurmoo, Chem. Soc. Rev. 38 (2009) 1353–1379.
[8] W. Xuan, C. Zhu, Y. Liu, Y. Cui, Chem. Soc. Rev. 41 (2012) 1677–1695.
[9] H. Furukawa, K.E. Cordova, M. O'Keeffe, O.M. Yaghi, Science 341 (2013) 1230444.
[10] J.J. Perry Iv, J.A. Perman, M.J. Zaworotko, Chem. Soc. Rev. 38 (2009) 1400–1417.
[11] M.P. Suh, H.J. Park, T.K. Prasad, D.W. Lim, Chem. Rev. 112 (2011) 782–835.
[12] A. Dhakshinamoorthy, M. Opanasenko, J. Čejka, H. Garcia, Adv. Synth. Catal. 355 (2013) 247–268.
[13] A. Corma, H. García, F.X. Llabrés i Xamena, Chem. Rev. 110 (2010) 4606–4655.
[14] K.K. Tanabe, S.M. Cohen, Angew. Chem. 121 (2009) 7560–7563.
[15] S. Hasegawa, S. Horike, R. Matsuda, S. Furukawa, K. Mochizuki, Y. Kinoshita, S. Kitagawa, J. Am. Chem. Soc. 129 (2007) 2607–2614.
[16] Z. Wang, S.M. Cohen, J. Am. Chem. Soc. 129 (2007) 12368–12369.
[17] Y. Song, L. Cronin, Angew. Chem. Int. Ed. 47 (2008) 4635–4637.
[18] Y.K. Hwang, D.Y. Hong, J.S. Chang, S.H. Jhung, Y.K. Seo, J. Kim, V. Alexandre, D. Marco, S. Christian, G. Férey, Angew. Chem. Int. Ed. 47 (2008) 4144–4148.
[19] C.P. Krap, R. Newby, A. Dhakshinamoorthy, H. García, I. Cebula, T.L. Easun, W. Lewis, Inorg. Chem. 55 (2016) 1076–1088.
[20] A. Dhakshinamoorthy, A.M. Asiri, H. Garcia, Catal. Sci. Technol. 6 (2016) 5238–5261.
[21] Maria N. Timofeeva, Valentina N. Panchenko, Nazmul Abedin Khan, Zubair Hasan, Igor P. Prosvirin, Sergey V. Tsybulya, Sung Hwa Jhung, Appl. Catal. A Gen. 529 (2017) 167–174.
[22] S.K. Lee, D.Y. Hong, M.G. Jeong, J.W. Yoon, J. Bae, Y.D. Kim, J.S. Chang, Microporous Mesoporous Mater. 253 (2017) 223–232.
[23] S.S.Y. Chui, S.M.F. Lo, J.P.H. Charmant, A.G. Orpen, I.D. Williams, Science 283 (1999) 1148–1150.
[24] M. Sasidharan, N. Gunawardhana, C. Senthil, M. Yoshio, J. Mater. Chem. A 2 (2014) 7337–7344.
[25] Y. Son, Y. Son, M. Choi, M. Ko, S. Chae, N. Park, J. Cho, Nano Lett. 15 (2015) 6914–6918.
[26] C. Avci, J. Ariñez-Soriano, A. Carné-Sánchez, V. Guillerm, C. Carbonell, I. Imaz, D. Maspoch, Angew. Chem. Int. Ed. 54 (2015) 14417–14421.
[27] M.S. Zielinski, J.W. Choi, T. La Grange, M. Modestino, S.M.H. Hashemi, Y. Pu, S. Birkhold, J.A. Hubbell, D. Psaltis, Nano Lett. 16 (2016) 2159–2167.
[28] J.S. Cho, J.M. Won, J.H. Lee, Y.C. Kang, Nanoscale 7 (2015) 19620–19626.
[29] X. Wu, W. Wang, N. Song, X. Yang, S. Khaimanov, N. Tsidaeva, Chem. Eng. J. 306 (2016) 382–392.
[30] T.S. Chadha, M. Yang, K. Haddad, V.B. Shah, S. Li, P. Biswas, Chem. Eng. J. 310 (2017) 102–113.
[31] P. Serra-Crespo, E.V. Ramos-Fernandez, J. Gascon, F. Kapteijn, Chem. Mater. 23 (2011) 2565–2572.

[32] D.Y. Hong, Y.K. Hwang, C. Serre, G. Ferey, J.S. Chang, Adv. Funct. Mater. 19 (2009) 1537–1552.
[33] T. Zhao, L. Yang, P. Feng, I. Gruber, C. Janiak, Y. Liu, Inorg. Chim. Acta 471 (2018) 440–445.
[34] F. Vermoortele, B. Bueken, G. Le Bars, B. Van de Voorde, M. Vandichel, K. Houthoofd, A. Vimont, M. Daturi, M. Waroquier, V.V. Speybroeck, C. Kirschhock, J. Am. Chem. Soc. 135 (2013) 11465–11468.
[35] Z. Wang, P. Fongarland, G. Lu, N. Essayem, J. Catal. 318 (2014) 108–118.
[36] F. Vermoortele, R. Ameloot, L. Alaerts, R. Matthessen, B. Carlier, E.V.R. Fernandez, J. Gascon, F. Kapteijn, D.E. De Vos, J. Mater. Chem. 22 (2012) 10313–10321.
[37] L. Mitchell, P. Williamson, B. Ehrlichová, A.E. Anderson, V.R. Seymour, S.E. Ashbrook, N. Acerbi, L.M. Daniels, R.I. Walton, M.L. Clarke, P.A. Wright, Chem. Eur. J. 20 (2014) 17185–17197.
[38] P. Serra-Crespo, E.V. Ramos-Fernandez, J. Gascon, F. Kapteijn, Chem. Mater. 23 (2011) 2565–2572.
[39] L. Gao, C.Y.V. Li, K.Y. Chan, Chem. Mater. 27 (2015) 3601–3608.
[40] Y. Wei, Y. Li, Y. Tan, Z. Wu, L. Pan, Y. Liu, Chem. Eng. J. 298 (2016) 271–280.
[41] G. Gómez- Pozuelo, C.P. Cabello, M. Opanasenko, M. Horáček, J. Čejka, ChemPlusChem 82 (2017) 152–159.
[42] M. Chen, J. Yan, Y. Tan, Y. Li, Z. Wu, L. Pan, Y. Liu, Ind. Eng. Chem. Res. 54 (2015) 11804–11813.
[43] X. Wu, X. Xia, Y. Chen, Y. Lu, RSC Adv. 6 (2016) 74028–74038.
[44] X. Wu, X. Xia, R. Liu, Y. Chen, RSC Adv. 6 (2016) 34625–34632.
[45] S.K. Jana, T. Kugita, S. Namba, Appl. Catal. A Gen. 266 (2004) 245–250.
[46] S.K. Jana, T. Okamoto, T. Kugita, S. Namba, Appl. Catal. A Gen. 288 (2005) 80–85.